#### Contents lists available at ScienceDirect

# **Mechanics Research Communications**

journal homepage: www.elsevier.com/locate/mechrescom



# Jeffery's paradox for the rotation of a single 'stick-slip' cylinder

Michael Siegel a,\*, Ehud Yariv b

- <sup>a</sup> Department of Mathematical Sciences, New Jersey Institute of Technology, Newark, 07102, NJ, USA
- b Department of Mathematics, Technion Israel Institute of Technology, Haifa, 32000, Israel

# ARTICLE INFO

Keywords: Superhydrophobic Stick-slip Stokes flow Stokes' paradox Jeffery's paradox

#### ABSTRACT

We consider the problem of determining the two-dimensional fluid velocity due to the rotation of an infinitelylong 'stick-slip' cylinder in an otherwise quiescent Stokes flow. Stick-slip boundary conditions are introduced as a model of a rough superhydrophobic surface, via a distribution of alternating solid-liquid (stick) and gas-liquid (slip) interfaces. This leads to a mixed boundary-value problem for Stokes flow. Complex variable techniques are employed to transform the flow problem into a Hilbert problem, which involves finding a function analytic in a plane region assuming that on some portions of the boundary its real part is known, while on others its imaginary part is given. We solve the Hilbert problem to obtain semi-analytic expressions for all the pertinent fluid-dynamic quantities. We find that in the general aperiodic case there is no solution in which the velocity of the fluid vanishes at infinity. This is a form of Jeffery's paradox, typically associated with viscous flow due to the counter-rotation of two equal rigid cylinders. Our work provides the first example of Jeffery's paradox due to the rotation of a single cylinder.

#### 1. Introduction

A superhydrophobic surface is a microstructured or rough hydrophobic solid that occurs in natural settings (e.g., the lotus leaf, butterfly wings, mosquito eyes) or is manufactured for applications [1, 2]. When immersed in a liquid, a stable configuration can form in which air is trapped within the vacancies of the microstructure; it is known as a Cassie state. This state tends to lead to reduced resistance for liquid motion over the surface, which is of great interest in technological applications [3].

Theoretical and numerical studies of liquid flow about superhydrophobic surfaces tend to concentrate on two classes of canonical problems. These are (i) externally imposed shear flow over a single surface, and (ii) pressure driven flow within a superhydrophobic channel. The main quantity of interest is a lumped or course-grained parameter that represents the reduced friction due to superhydrophobicity. In (i), this quantity is the intrinsic slip length [4-6], which depends solely on the detailed surface geometry. In (ii), the relevant quantity is the excess volumetric flux compared to that for a channel with rigid walls [7]. Recently, experiments [8–10] have explored a third class of flows, namely, that due to the rigid-body motion of a superhydrophobic particle. In this class, the lumped parameter of interest is the enhancement in particle mobility.

Perhaps the simplest resistance problem for the rigid-body motion of a particle in a viscous liquid is rotation of an infinite circular cylinder about its axis. For that problem, superhydrophobicity is established by introducing an arrangement of air-filled grooves parallel to the cylinder axis, separated by solid ridges (see Fig. 1). The grooves present a shearfree or 'slip' boundary to the liquid flow, which alternates with the no-slip or 'stick' boundary at the solid ridges. Yariv and Siegel [11] considered a periodic arrangement of N equal-sized liquid-gas interfaces separated by N equal-sized solid-liquid interfaces at arbitrary solid fraction  $\phi$  (where the liquid-air interface may have a different size from a solid-liquid one). We refer to this as a 'periodic' geometry. The ratio M of the rotational mobility to the respective mobility of a homogeneous cylinder then depends only on N and  $\phi$ . Using a nonconventional approach, where information from a conformal-mapping procedure is combined with that from an asymptotic expansion for  $N \gg 1$ , [11] derive a simple exact expression

$$M = 1 - \frac{2}{N} \log \left( \sin \left( \frac{\pi \phi}{2} \right) \right) \tag{1}$$

for the mobility. This result was obtained without solving for the detailed fluid flow.

The current paper has two main objectives. One is to extend the complex variable approach introduced in [11] to find solutions for all the pertinent fluid dynamic quantities. This is done by transforming the flow problem into a Hilbert problem, which involves determining an analytic function in the region exterior to the cylinder when its real part is given on some sections of the boundary, while its imaginary part is given on others. We solve the Hilbert problem to obtain semianalytic expressions for all the relevant flow quantities, allowing for

Available online 21 June 2023

Corresponding author. E-mail address: misieg@njit.edu (M. Siegel).

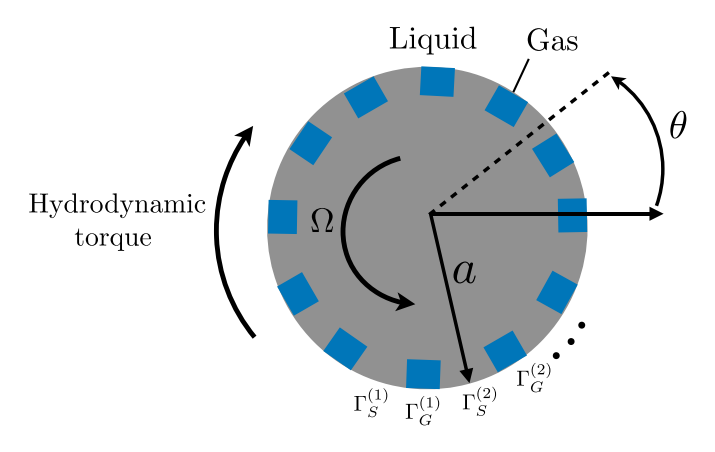


Fig. 1. Schematic of the geometry. Grooves  $\Gamma_G^{(k)}$  with trapped gas bubbles alternate with solid surfaces  $\Gamma_S^{(k)}$  for k = 1, 2, ...

the general case of aperiodic arrangement of grooves. Our approach is related to that employed in [12] for a different physical problem involving drop deformation with surfactant. An alternative approach that also applies to this class of mixed boundary-value problems is given by Crowdy [13].

The second objective is to show that, in the case of an aperiodic distribution of grooves, there is in general no solution to the problem in which the velocity of the fluid vanishes at infinity. This is a form of the Jeffery's paradox, which is traditionally associated with the counterrotation of two equal infinite cylinders [14,15]. Here, we find that the fluid velocity due to the steady rotation of a single aperiodic stick-slip cylinder tends to a uniform flow at infinity. Our work provides the first example of Jeffery's paradox due to the purely rotational motion of a single cylinder.

#### 2. Governing equations

We consider an infinitely-long solid cylinder of radius a patterned with  $N \ge 1$  grooves, which are of infinite length in the axial direction. The periodic geometry in the case of equally-sized and uniformlyspaced grooves is shown in Fig. 1. (We do not require the geometry to be periodic.) The cylinder is immersed in a liquid of viscosity  $\mu$  and is assumed to attain a stable Cassie state, so that a gas bubble is trapped in each groove. The boundary of the cylinder therefore consists of an alternating array of liquid-gas interfaces (bubbles) and liquid-solid interfaces (solid ridges which separate the bubbles). We further assume (cf. [7]) that the surface has the constant curvature 1/a, so that the curvature of the liquid-gas interfaces coincides with that of the solid ridges. Their union is accordingly a circle of radius a. Denote the solid fraction of the compound boundary by  $\phi$ , which satisfies  $0 \le \phi \le 1$ .

A two-dimensional flow is generated by an imposed rotation of the cylinder about its axis with angular velocity  $\Omega$ . We seek to ascertain the flow, its associated rotational mobility M and the velocity at infinity. The latter two quantities must also be determined as part of the solution.

The governing equations are presented in dimensionless form using a,  $a\Omega$  and  $\mu\Omega$  as the units of length, velocity, and stress, respectively. We employ a fixed reference frame using (x, y, z) Cartesian coordinates, with the z-axis coinciding with the cylinder axis. We also make use of  $(r, \theta)$  polar coordinates in the xy-plane, where r is distance from the *z*-axis and  $\theta$  is the angle with respect to the *x*-axis.

Denote the fluid region by  $\mathcal{D}$ , and introduce the sets  $\Gamma_S$  and  $\Gamma_G$ in which  $\theta \in \Gamma_S$  (respectively  $\Gamma_G$ ) if  $\theta$  is on the solid (respectively shear-free or groove) part of the boundary r=1. These sets each consist of N disjoint intervals  $\Gamma_S^{(k)}$  and  $\Gamma_G^{(k)}$  for  $k=1,\ldots,N$ , so that  $\Gamma_S=\bigcup_{k=1}^N\Gamma_S^{(k)}$  and  $\Gamma_G=\bigcup_{k=1}^N\Gamma_S^{(k)}$  (see Fig. 1). The velocity field  $\mathbf{u}(r,\theta) = u(r,\theta)\hat{\mathbf{e}}_{\mathbf{r}} + v(r,\theta)\hat{\mathbf{e}}_{\theta}$  in  $\mathcal{D}$  satisfies the Stokes and continuity

$$\frac{\partial p}{\partial r} = \nabla^2 u - \frac{u}{r^2} - \frac{2}{r^2} \frac{\partial v}{\partial \theta}, \quad \frac{1}{r} \frac{\partial p}{\partial \theta} = \nabla^2 v + \frac{2}{r^2} \frac{\partial u}{\partial \theta} - \frac{v}{r^2}, \quad \frac{\partial (ru)}{\partial r} + \frac{\partial v}{\partial \theta} = 0, \quad (2)$$

where p is the pressure. The boundary conditions at r = 1 are the no-penetration condition u = 0 and the mixed no-slip and shear-free

$$v = 1$$
 for  $\theta \in \Gamma_S$ ,  $\frac{\partial v}{\partial r} - \frac{v}{r} = 0$  for  $\theta \in \Gamma_G$ . (3)

Normalized by  $4\pi\mu a^2\Omega$ , the hydrodynamic torque on the cylinder in the counterclockwise direction is

$$T = -\frac{1}{4\pi} \int_0^{2\pi} \left[ r^2 \left( \frac{\partial v}{\partial r} - \frac{v}{r} \right) \right]_{r=1} d\theta. \tag{4}$$

It may be evaluated over any cylindrical surface enclosing the unit cylinder. In particular, the large-r asymptotic expansion of  $\mathbf{u}$  must include a rigid-body-rotation mode,  $(T/r)\hat{\mathbf{e}}_{\theta}$ . By subtracting off that mode, we define the excess velocity

$$\dot{\mathbf{u}} = \mathbf{u} - \frac{T}{r} \hat{\mathbf{e}}_{\theta},\tag{5}$$

where  $\dot{\mathbf{u}} = \dot{u}\hat{\mathbf{e}}_{\mathbf{r}} + \dot{v}\hat{\mathbf{e}}_{\theta}$ . The value of the torque depends on the surface morphology and is determined as part of the solution from the requirement that the excess field (5) is torque-free. Note that T = 1 for a homogeneous cylinder, where  $\phi = 1$ .

Just as for the torque, the far-field boundary condition on  $\dot{\mathbf{u}}$  is not specified, but is rather determined as part of the solution. We single out a unique solution by picking out the one which is least singular as

#### 3. Complex variable formulation

Define a streamfunction  $\grave{\psi}$  associated with the excess velocity  $\grave{\textbf{u}}$  as  $\dot{\mathbf{u}} = \nabla \dot{\boldsymbol{\psi}} \times \hat{\mathbf{e}}_{\tau}$ 

The streamfunction satisfies the biharmonic equation in  $\mathcal{D}$ . The no penetration boundary condition implies that  $\dot{\psi}$  is constant on r=1, which is taken to be zero. The mixed boundary condition at r = 1 (cf.

$$\frac{\partial \dot{\psi}}{\partial r} = T - 1 \text{ for } \theta \in \Gamma_S$$

$$\begin{split} \frac{\partial \dot{\psi}}{\partial r} &= T - 1 \ \text{ for } \theta \in \varGamma_S, \\ \frac{\partial^2 \dot{\psi}}{\partial r^2} &- \frac{\partial \dot{\psi}}{\partial r} &= -2T \ \text{ for } \theta \in \varGamma_G. \end{split}$$

We now employ the Goursat representation for biharmonic functions [16].

$$\hat{\psi} = \operatorname{Re}\left\{\bar{\zeta}f(\zeta) + g(\zeta)\right\},\tag{6}$$

where  $\zeta = x + iy$ , and  $f(\zeta)$  and  $g(\zeta)$  are analytic functions in the fluid region  $|\zeta| > 1$ . The overbar denotes complex conjugate. We use the notation  $h(\theta)$  to denote evaluation of a function  $h(\zeta)$  on the boundary  $\zeta = e^{i\theta}$ .

The vanishing of  $\dot{\psi}$  on the cylinder boundary implies that the streamfunction has the representation

$$\dot{\psi} = \operatorname{Re}\left\{ \left( \xi - \frac{1}{\zeta} \right) G(\zeta) \right\},$$
(7)

where  $G(\zeta)$  is analytic in  $|\zeta| > 1$ . Comparing (6) and (7), we identify  $f(\zeta)$  with  $G(\zeta)$ , and  $g(\zeta)$  with  $-G(\zeta)/\zeta$ . All pertinent fluid dynamic quantities, such as the velocity and pressure in D, can be determined from knowledge of the Goursat functions [17].

The mixed no-slip and zero shear stress boundary condition is written in terms of the single function G by substituting  $\zeta = re^{i\theta}$  into (7) and taking r-derivatives of  $\hat{\psi}$  to find on r = 1,

$$2\operatorname{Re}\left\{\frac{G(e^{i\theta})}{e^{i\theta}}\right\} = T - 1 \text{ for } \theta \in \Gamma_S,$$
(8)

$$4\operatorname{Re}\left\{\frac{G(e^{i\theta})}{e^{i\theta}}-G_{\zeta}(e^{i\theta})\right\} = 2T \text{ for } \theta \in \Gamma_G, \tag{9}$$

where the  $\zeta$  subscript denotes differentiation with respect to the argument. For later use, we note that

$$\hat{u} = \left(r - \frac{1}{r}\right) \operatorname{Im} \left\{ \frac{G(re^{i\theta})}{re^{i\theta}} - G_{\zeta}(re^{i\theta}) \right\},$$
(10)

$$\dot{v} = -\left(r + \frac{1}{r}\right) \operatorname{Re} \left\{ \frac{G(re^{i\theta})}{re^{i\theta}} \right\} - \left(r - \frac{1}{r}\right) \operatorname{Re} \left\{ G_{\zeta}(re^{i\theta}) \right\}, \tag{11}$$

throughout  $\mathcal{D}$ . On the boundary we write

$$\frac{G(\zeta)}{\zeta} = U + iV \quad \text{for} \quad \zeta = e^{i\theta},\tag{12}$$

where U and V are real. Then it is easily seen that the boundary conditions (8)–(9) on r=1 are equivalent to

$$U = \frac{T-1}{2} \text{ for } \theta \in \Gamma_S, \tag{13}$$

$$\frac{\partial V}{\partial \theta} = -\frac{\bar{T}}{2} \text{ for } \theta \in \Gamma_G.$$
 (14)

Integrating (14), we find that on r = 1

$$V = T\left(C_k - \frac{1}{2}\theta\right) \text{ for } \theta \in \Gamma_G^{(k)},\tag{15}$$

where  $C_k$  (k = 1, ..., N) is a constant.

The problem has therefore been transformed into the Hilbert problem: to determine a function (namely,  $G(\zeta)/\zeta$ ) which is analytic in the region  $\mathcal{D}$ , with its real part given on some portion of the boundary, and its imaginary part given on the remaining portion. We ask for a solution satisfying the physical requirement that the tangential excess velocity on the cylinder, which per (11)–(12) is  $\dot{v}=-2U$ , is continuous in  $\theta$  on r=1.

Using the Poisson Integral Formula [16], we can express the analytic function  $G(\zeta)/\zeta$  for  $|\zeta| > 1$  in terms of an integral:

$$\frac{G(\zeta)}{\zeta} = -\frac{1}{2\pi i} \oint_{|\zeta'|=1} \frac{d\zeta'}{\zeta'} \frac{\zeta' + \zeta}{\zeta' - \zeta} U(\zeta') + iK, \tag{16}$$

where K is a real constant, and the contour is taken in the counterclockwise direction. This provides a representation of the solution in  $\mathcal{D}$  in terms of an unknown 'density'  $U(\zeta)$  on  $|\zeta|=1$ . We use an additional degree of freedom, associated with the unknown torque T, to require that the velocity be at least bounded at infinity. (It will be seen that the velocity cannot in general be made to decay to zero at infinity.) From (7), a bounded velocity implies that  $G(\zeta)/\zeta \to 0$  at  $\zeta \to \infty$ . Enforcing this by taking the limit  $\zeta \to \infty$  in (16) gives

$$\int_{0}^{2\pi} U(\theta') \ d\theta' = 0,\tag{17}$$

$$K = 0. (18)$$

Later, the condition (17) will be employed to obtain an expression for the torque.

To obtain an equation for the density U, let  $\zeta \to t = e^{i\theta}$  in (16), substitute  $\zeta' = e^{i\theta'}$  and use the Plemelj formula and (18) to find that

$$\begin{split} \frac{G(t)}{t} &= -\frac{1}{2\pi i} \operatorname{PV} \int_0^{2\pi} U(\theta') \cot\left(\frac{\theta' - \theta}{2}\right) d\theta' + U(\theta), \\ & \text{for } t = e^{i\theta} \text{ and } \theta \in [0, 2\pi], \end{split}$$

 $= i\mathcal{H}[U](\theta) + U(\theta),$ 

where PV denotes Cauchy principal value integral, and we have introduced the periodic Hilbert transform  $\mathcal{H}[f]$ , defined by

$$\mathcal{H}[f] = \frac{1}{2\pi} \operatorname{PV} \int_0^{2\pi} f(\theta') \cot\left(\frac{\theta' - \theta}{2}\right) d\theta'. \tag{19}$$

It immediately follows that

$$V(\theta) = \mathcal{H}[U](\theta), \text{ for } \theta \in [0, 2\pi],$$
 (20)

which is the usual relationship between the real and imaginary parts of a function that is analytic in the exterior of a unit disk.

Next, introduce a modified 'density' function

$$T\hat{U}(\theta) = U(\theta) - \frac{T-1}{2},\tag{21}$$

which in view of (13) is zero for  $\theta \in \Gamma_S$ . To obtain an equation for  $\hat{U}(\theta)$  on  $\Gamma_G$ , substitute (21) into (20) and make use of (15) and the fact that the Hilbert transform of a constant is zero to obtain

$$\frac{1}{2\pi} \operatorname{PV} \int_{\Gamma_G} \hat{U}(\theta') \cot \left( \frac{\theta' - \theta}{2} \right) d\theta' = B_k(\theta) \text{ for } \theta \in \Gamma_G^k, \ k = 1, \dots, N,$$
(22)

where

$$B_k(\theta) = C_k - \theta/2 \tag{23}$$

for constant  $C_{k}$ .

The above integral equation for  $\hat{U}(\theta)$  is the main result of this section. We make two important remarks about this equation. First, the principal value integral in (22) is not a Hilbert transform, since the integration interval differs from  $[0,2\pi]$ . Therefore, the usual formula for the inversion of the Hilbert transform does not apply. Second, continuity of  $U(\theta)$  implies that  $\hat{U}(\theta) \to 0$  as  $\theta$  tends to the endpoints of each interval  $\Gamma_G^{(k)}$  for  $k=1,\ldots,N$ . Thus, the principal value integral is well defined at these points.

In the next two sections, we write down solutions for  $\hat{U}(\theta)$  (first for N=1 and then for N>1) from which all the relevant flow quantities can be obtained. We also discuss the far-field velocity and Jeffery's paradox for our problem.

#### 4. Solution of Hilbert's problem for N = 1

We first consider the case N=1, in which the cylinder has one groove. The solution is extended to N>1 in Section 5.

A particular solution to (22) can be found for N=1 following [16]. First assume, with no loss of generality, that the groove or shear-free part of the boundary is instantaneously located at  $\Gamma_G = [\theta_m - \theta_0, \theta_m + \theta_0]$ , where  $\theta_m$  is the groove midpoint and  $0 < \theta_0 < \pi$ . Let  $\tilde{\theta} = \theta_m + \theta_0$  be the right endpoint of  $\Gamma_G$ , and set  $\alpha = e^{i\tilde{\theta}}$  so that the groove boundary is the arc between  $\zeta = -\bar{\alpha}$  and  $\alpha$ , taken counterclockwise (see Fig. 4). Introduce

$$\omega(\zeta) = \left(\frac{\zeta - \alpha}{\zeta + \bar{\alpha}}\right)^{1/2},\tag{24}$$

with branch cuts chosen to lie along the surface contour corresponding to  $\Gamma_G$ . In the appendix it is shown that a particular solution to (22) is given by the integral formula

$$\hat{U}_p(\theta) = \text{PV} \int_{\Gamma_G} K(\theta, \theta') \cot \left( \frac{\theta' - \theta}{2} \right) \ d\theta' \ \text{ for } \theta \in \Gamma_G, \tag{25}$$

where

$$K(\theta, \theta') = -\frac{1}{4\pi} \left[ \frac{\omega(\theta)B(\theta')}{\omega(\theta')} + \frac{\omega(\theta')B(\theta')}{\omega(\theta)} \right]. \tag{26}$$

and  $B(\theta)$  is given by (23). (For convenience we have omitted the subscript 1 on  $B_1$ .) It is easily verified that this expression for  $\hat{U}_p(\theta)$  is real-valued. A required symmetry of this solution is that the  $\theta$ -component of the excess velocity,  $\hat{v}(\theta)$ , is even about the midpoint of the groove  $\theta_m$ . It follows from (11) and (12) that U and  $T\hat{U} = U - (T-1)/2$  are even about  $\theta_m$ , and from (22) that  $B(\theta)$  is odd about  $\theta_m$ . This odd symmetry determines the unknown constant  $C_1$  in (23) to be  $\theta_m/2$ , so that

$$B(\theta) = \frac{1}{2} \left( \theta_m - \theta \right) = \frac{1}{2} \left( \frac{3\pi}{2} - \theta \right) \tag{27}$$

where, without loss of generality, we have chosen  $\theta_m = 3\pi/2$ .

The particular solution  $\hat{U}_p(\theta)$  has a singularity of the form  $c(\theta-\tilde{\theta})^{-1/2}$  as  $\theta$  approaches the endpoint  $\tilde{\theta}$  where boundary conditions change type, and an analogous singularity at the other endpoint of  $\Gamma_G$ . The

fluid velocity associated with  $\hat{U}_p$  generates nonintegrable stress singularities at these points, which is unphysical. To remove the singularities, we add a solution  $\hat{U}_h$  of the homogeneous version of (22)

$$\frac{1}{2\pi} \operatorname{PV} \int_{\Gamma_G} \hat{U}(\theta') \cot \left( \frac{\theta' - \theta}{2} \right) d\theta' = 0 \text{ for } \theta \in \Gamma_G,$$
 (28)

to  $\hat{U}_p(\theta)$ , so that the leading-order singularities cancel out. This will uniquely determine the solution to our problem.

The homogeneous solution is derived in the Appendix (Section A.2) and takes the form

$$\hat{U}_{h}(\theta) = Q \frac{e^{i\theta} - i}{\left[ (e^{i\theta} - \alpha)(e^{i\theta} + \tilde{\alpha}) \right]^{1/2}} \text{ for } \theta \in \Gamma_{G},$$
(29)

where Q is a constant which is taken to be real to ensure that  $\hat{U}_h$  is real (one can check that  $\overline{\hat{U}}_h = \hat{U}_h$ ). Note that  $\hat{U}_h(\theta)$ , like  $\hat{U}_p(\theta)$ , is an even function of  $\theta$  about  $\theta_m$ . Thus, the leading order singularity at each endpoint of  $\Gamma_G$  can be removed by appropriate choice of the single parameter Q. When  $\theta \in \Gamma_G$  is near  $\hat{\theta}$  the leading-order singular behavior of  $\hat{U} = \hat{U}_p + \hat{U}_h$  is found to be

$$\hat{U}(\theta) \sim i \left[ -\frac{1}{4\pi} (\alpha + \bar{\alpha})^{1/2} J(\tilde{\theta}) + Q \frac{\alpha - i}{(\alpha + \bar{\alpha})^{1/2}} \right] (\theta - \tilde{\theta})^{-1/2},$$

where  $J(\theta)$  is given by

$$J(\theta) = \text{PV} \int_{\Gamma_G} B(\theta') \omega(\theta') \cot\left(\frac{\theta' - \theta}{2}\right) d\theta', \text{ for } \theta \in \Gamma_G.$$
 (30)

Note that  $J(\tilde{\theta})$  is well defined since  $\omega(\theta)$  tends to zero as  $\theta \to \tilde{\theta}$ . We remove the leading order singularity by setting the expression within brackets to zero to obtain

$$Q = \frac{1}{4\pi} \left( \frac{\alpha + \bar{\alpha}}{\alpha - i} \right) J(\tilde{\theta}). \tag{31}$$

It can be analytically verified that  $J(\tilde{\theta})/(\alpha-i)$  is real valued. This completes our determination of the homogeneous solution.

It only remains to determine the torque. An expression for T is readily obtained by substituting  $U(\theta) = (T-1)/2 + T\hat{U}(\theta)$  (cf. (21)) into the condition (17) and solving for T, which gives

$$T = \frac{\pi}{\pi + \mathcal{I}(\phi)}. (32)$$

where

$$I(\phi) = \int_{\Gamma_G} \hat{U}(\theta') \ d\theta'. \tag{33}$$

In the above, we have used  $\hat{U}(\theta) = 0$  for  $\theta \notin \Gamma_G$ . The notation  $\mathcal{I}(\phi)$  is chosen to emphasize that this quantity depends only on the solid fraction  $\phi$ .

Summarizing, Eqs. (25), (29), (31), and (32) provide an explicit representation for the solution U in terms of principal value integrals of *known* functions:

$$U(\theta) = (T - 1)/2 + T\hat{U}(\theta) \text{ where}$$
(34)

$$\begin{split} \hat{U}(\theta) &= \hat{U}_p(\theta) + \hat{U}_h(\theta) = -\operatorname{PV} \int_{\Gamma_G} K(\theta, \theta') \cot \left(\frac{\theta' - \theta}{2}\right) \ d\theta' \\ &+ \frac{J(\tilde{\theta})}{4\pi} \left(\frac{\alpha + \bar{\alpha}}{\alpha - i}\right) \frac{e^{i\theta} - i}{\left[(e^{i\theta} - \alpha)(e^{i\theta} + \bar{\alpha})\right]^{1/2}}, \end{split} \tag{35}$$

for  $\theta \in \Gamma_G$ , while  $U(\theta) = (T-1)/2$  for  $\theta \in \Gamma_S$ , per (13). Here we recall that  $\alpha$  is defined in Fig. 4, and explicit formulas for  $\omega(\theta)$ ,  $B(\theta)$ ,  $J(\theta)$  and T are given by (24), (27), (30), and (32). This completes our explicit solution in the case of a single groove. The fluid velocity in D can be determined from the above formula for  $U(\theta)$ , via (10), (11), and (16). Critically, the velocity is uniquely determined, and there are no remaining free parameters which can be used to control the velocity at infinity. We will see that in general, the velocity does not decay to zero at infinity, which is a form of Jeffery's paradox.

We are unable to analytically evaluate the singular integrals in (35), but they are readily computed numerically using an adaptation of the method in [12]. We provide a brief description of the numerical

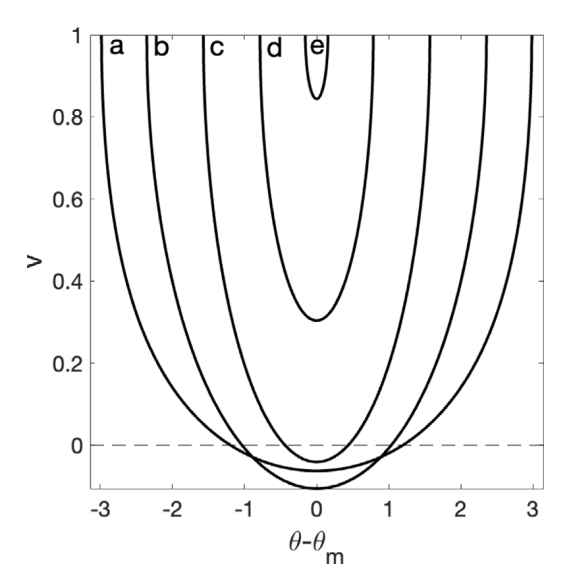


**Fig. 2.** Surface velocity  $v(\theta)$  for N=1 at different solid fractions. (a)  $\phi=1/20$ , (b) 1/4, (c) 1/2, (d) 3/4, and (e) 19/20.

method. When  $\theta \in \Gamma_G$  is on the shear-free part of the boundary, there is a pole singularity in the integrand at  $\theta' = \theta$ . This is removed by a standard method of singularity subtraction, which gives an integrand that is analytic at points in the interior of  $\Gamma_G$ . However, there are still inverse-square-root kernel singularities at the endpoints of  $\Gamma_G$ . The hybrid Gauss-trapezoid quadrature of Alpert [18] is applied to the desingularized integrand to accurately handle these endpoint singularities, improving on the simpler but less accurate method employed in [12]. Alpert's method can be implemented with arbitrarily high-order accuracy, and we choose a fourth-order version. Resolution studies and comparison with exact formula (cf. Section 5.1) show the method gives accurate results for velocities close to the stick–slip points, and for solid fractions  $\phi$  that are either very small or near 1, which are typically delicate to resolve.

It is instructive to plot some physical quantities for the case N=1. A plot of the surface velocity  $v(\theta)$  for  $\theta \in \Gamma_G$  and different solid fractions is shown in Fig. 2. This velocity has square-root singularities at the two endpoints of the shear-free region  $\Gamma_G$ , which is the canonical singularity at a stick–slip point [12,19]. Below a critical solid fraction, there are two stagnation points at the boundary with reversed flow between them. The minimum  $v(\theta)$  or largest magnitude reversed flow occurs when  $\phi$  is about 0.27, which is close to the case plotted in (b) of Fig. 2.

Let  $\psi = -T \ln r + \dot{\psi}$  denote the streamfunction corresponding to the physical velocity **u**. The flow streamlines  $\psi = \text{const}$  are shown for two different solid fractions in Fig. 3. For  $\phi = 0.5$  (Fig. 3(a)), there is a pair of stagnation points on the boundary; see also Fig. 2, curve (c). The streamlines that pass through these stagnation points divide the flow into two sets of open streamlines: an 'upper' set in which the flow is in the counterclockwise direction, and a 'lower' set where the flow is reversed, i.e., in the clockwise direction. As the solid fraction is increased the boundary stagnation points approach each other and collide at  $\theta = 3\pi/2$ , after which (for yet larger solid fraction) a single stagnation point detaches from the boundary and moves into the fluid interior. The topology of the streamlines then changes, as shown in Fig. 3(b). There is a set of closed streamlines surrounding the cylinder corresponding to counterclockwise flow. Further out, there are two sets of open streamlines, corresponding to counterclockwise flow far above the cylinder and clockwise motion far below. The streamline pattern indicates a streaming motion at infinity.

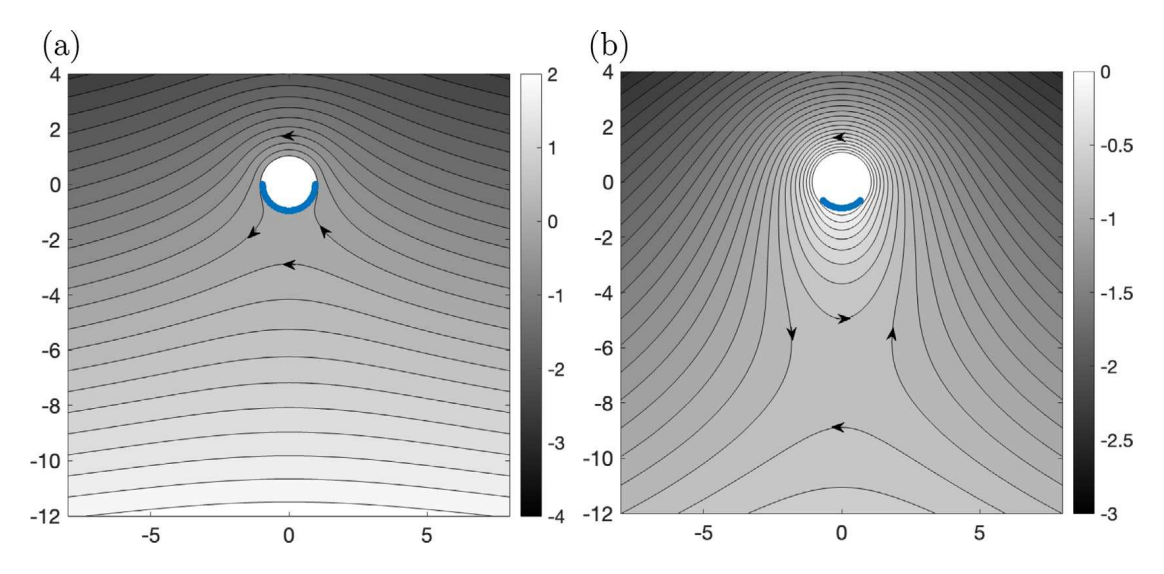


Fig. 3. Streamlines  $\psi = \text{const}$  due to counterclockwise rotation of the cylinder. The gas-liquid interface is shown in blue. (a)  $\phi = 0.5$  ( $A_{\phi} = -0.295$ ), (b)  $\phi = 0.75$  ( $A_{\phi} = -0.126$ ). The nonzero value of  $A_{\phi}$  implies the velocity does not decay to zero at infinity, which is a form of Jeffery's paradox.

#### 4.1. Jeffery's paradox

We compute the far-field velocity by expanding  $G(\zeta)$  for large  $\zeta$ using (16), and simplify by employing the even symmetry of  $U(\theta)$  about  $\theta_m = 3\pi/2$  to find that

$$G(\zeta) \sim \frac{i}{\pi} \int_0^{2\pi} U(\theta') \sin \theta' \ d\theta' \ \text{as} \ \zeta \to \infty.$$

It follows from (10), (11) that the radial and tangential excess velocity as  $r \to \infty$  satisfy

$$\dot{u} \sim A_{\phi} \cos \theta, \quad \dot{v} \sim -A_{\phi} \sin \theta,$$
(36)

where for the assumed cylinder orientation

$$A_{\phi} = \frac{1}{\pi} \int_0^{2\pi} U(\theta') \sin \theta' \ d\theta', \tag{37}$$

which depends only on the solid fraction  $\phi$ . When N=1, the value of  $A_{\phi}$  is nonzero for all  $\phi \in (0,1)$  and tends to zero as  $\phi \to 0$  or 1. Thus, the velocity does not decay to zero at infinity for  $\phi \neq 0, 1$ . This is Jeffery's paradox for the problem with N = 1.

In Cartesian coordinates, the far-field velocity (36) is a uniform streaming motion  $\mathbf{u} = (A_{\phi}, 0)$  as can be seen in Fig. 3. We have crossvalidated (36) by numerically solving for  $\psi$  using a dual Fourier series approach in the spirit of Lauga and Stone [7]. This gives a far-field velocity that numerically agrees with (36).

# 5. Solution for N > 1 uniformly-spaced grooves

One can generalize the solution in Section 4 to N grooves of arbitrary size and spacing, separated by N arbitrarily-sized solid boundaries. This is done in the appendix. We presently find it more instructive to develop a class of periodic solutions with N > 1 equal-sized and uniformly-spaced grooves. These solutions are obtained from that for N = 1 using conformal mapping.

We illustrate the periodic solution for N = 2. Introduce a conformal map from the  $\zeta$ -plane to the upper-half z-plane, taking the branch cut to go through the groove midpoint at  $\theta_m$ . When  $\theta_m = 3\pi/2$ , the map is given by  $z(\zeta) = \sqrt{i\zeta}$  where  $\sqrt{\zeta} = r^{1/2}e^{i\theta/2}$  and  $-\pi/2 < \theta < 3\pi/2$  (see Fig. 4). Let  $z = r_z e^{i\theta_z}$  and define

$$U_2(\theta) = (T - 1)/2 + T\hat{U}(\theta)/2, \tag{38}$$

$$\begin{split} U_{2}(\theta) &= (T-1)/2 + T\hat{U}(\theta)/2, \\ G_{2}(z) &= -\frac{z}{2\pi i} \oint_{|\zeta'|=1} \frac{d\zeta'}{\zeta'} \frac{\zeta' + \zeta(z)}{\zeta' - \zeta(z)} U_{2}(\zeta'), \end{split} \tag{38}$$

where  $\zeta(z) = -iz^2$  and recall  $\hat{U}$  is given by (35) for  $\theta \in \Gamma_G$ , and is zero for  $\theta \in \Gamma_S$ . Eq. (38) defines a rescaled density on the unit circle in the  $\zeta$ -plane (compare to (34)), and (39) defines  $G_2(z)$  in the upper-half z-plane exterior to the unit disk. The function  $G_2(z)$  can be periodically extended to the whole z-plane exterior to the unit disk, with Morera's theorem guaranteeing analyticity there (equivalently,  $G_2$ can be analytically extended using the Schwarz reflection principle). Then on  $z = e^{i\theta_z}$ , (39) and the Poisson integral formula imply that

$$\frac{G_2(z)}{z} = U_2 + iV_2, (40)$$

which periodically extends the real function  $U_2$  to the unit circle in the *z*-plane, and defines the real function  $V_2(\theta_z) = \mathcal{H}[U_2](\theta_z)$ .

By construction, the functions  $U_2$  and  $V_2$  in (40) satisfy

$$U_2(\theta_z) = \frac{T-1}{2} \text{ for } \theta_z \in \Gamma_S^z$$
 (41)

$$\frac{\partial V_2}{\partial \theta_z}(\theta_z) = -\frac{T}{2} \text{ for } \theta_z \in \Gamma_G^z. \tag{42}$$

where  $\Gamma_S^z$  and  $\Gamma_G^z$  represent the solid and groove regions in the z-plane after mapping and reflection. To see this, note that  $\hat{U}_2 = 0$  for  $\theta_z \in \Gamma_S^z$ which shows (38) satisfies (41). Eq. (42) follows from noting that for  $\theta_z \in \Gamma_G^z$ ,  $V_2(\theta_z) = \frac{1}{2}V(\theta)$  with  $\theta = 2\theta_z - \pi/2$ , so that  $\partial V_2/\partial \theta_z = \partial V/\partial \theta = \pi/2$ -T/2, per (14). Now define the streamfunction

$$\dot{\psi}_2 = \left(\bar{z} - \frac{1}{z}\right) G_2(z). \tag{43}$$

Comparing (41), (42) with (13), (14), we see that  $G_2(z)/z$  solves the Hilbert problem in the z-plane, and thus  $\psi_2$  is a solution of the problem for N=2.

The square-root map can be generalized to  $z(\zeta) = (i\zeta)^{1/N}$  for integer N > 1, and a straightforward extension of the above procedure gives the solution in the exterior of the unit disk in the z-plane for N equallyspaced and sized grooves (an illustration of the N=4 geometry is shown Fig. 4c). If we let  $\theta_z = 0$  correspond to the midpoint of a groove, then the N-groove solution is written over a single period  $0 \le \theta_z < 2\pi/N$  (i.e., a sector between midpoints of adjacent grooves)

$$U_{N}(\theta_{z}) = \begin{cases} \frac{T-1}{2} + \frac{T\hat{U}(N\theta_{z} - \pi/2)}{N}, & 0 \le \theta_{z} < \frac{\theta_{0}}{N}, \\ \frac{T-1}{2}, & \frac{\theta_{0}}{N} \le \theta_{z} < \frac{2\pi - \theta_{0}}{N}, \\ \frac{T-1}{2} + \frac{T\hat{U}(N\theta_{z} - \pi/2)}{N}, & \frac{2\pi - \theta_{0}}{N} \le \theta_{z} \le \frac{2\pi}{N}, \end{cases}$$
(44)

where  $\hat{U}(\theta)$  is the N=1 solution from Section 4, and we recall that  $\theta = N\theta_z - \pi/2$ . The density  $U_N(\theta_z)$  can be periodically extended to

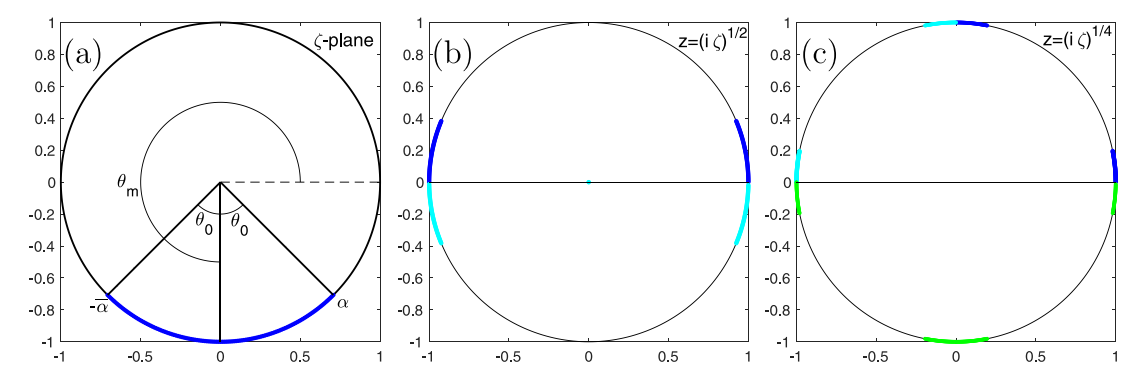


**Fig. 4.** (a) The cylinder in the ζ-plane for N = 1. The groove midpoint is  $\theta = \theta_m$ ; other quantities are defined in the text. (b) N = 2 geometry generated by the mapping  $z = (i\zeta)^{1/2}$ . The groove boundary is mapped into the upper unit semi-circle, and is extended into the lower semi-circle upon Schwarz reflection. (c) N = 4 geometry after a second mapping and Schwarz reflection.

 $\theta_z \in [0,2\pi].$  Physical quantities (e.g., the velocity) in the z-plane are obtained from

$$\dot{\psi}_N = \left(\bar{z} - \frac{1}{z}\right) G_N(z),$$

$$G_N(z) = -\frac{z}{2\pi i} \oint_{|\zeta'|=1} \frac{d\zeta'}{\zeta'} \frac{\zeta' - iz^N}{\zeta' + iz^N} U_N(\zeta'),$$
(45)

where we recall  $\zeta = e^{i\theta}$ . These are the *N*-groove analogues of (39), (43).

The torque T can now be obtained by inserting (44) into the condition (17). After changing integration variable to  $\theta$ , we find that

$$T = \frac{\pi}{\pi + I(\phi)/N}$$
 for  $N = 1, 2, ...$  (46)

where the quantity I is exactly the same as that in (33), i.e., independent of N. The corresponding mobility is

$$M = 1 + \frac{\mathcal{I}(\phi)}{N\pi}.\tag{47}$$

#### 5.1. Relation to large N asymptotics

Yariv and Siegel [11] were able to glean the 1/N scaling of M-1 in (47) without solving for the fluid velocity. Then, comparing (47) with a two term asymptotic expansion for the mobility in the limit  $N\gg 1$ , they concluded that

$$I(\phi) = -2\pi \log \left(\sin \left(\pi \phi/2\right)\right),\tag{48}$$

which together with (47) yields the exact expression (1). Formula (48) agrees to high precision with numerical evaluation of  $\mathcal{I}(\phi)$  using (33), (35).

#### 6. Remarks on Jeffery's paradox for N > 1

The far-field limit of the excess velocity for the periodic N-groove solution constructed in Section 5 can be computed by taking the limit  $z\to\infty$  in (39). It is readily seen that

$$\dot{\mathbf{u}} = O(r^{1-N}) \quad \text{as} \quad r \to \infty,$$
(49)

which decays to zero when  $N \ge 2$ . Hence there is no Jeffery paradox associated with these periodic solutions. However, the decay depends on an essential way on the symmetry. Roughly speaking, the far-field streaming motion induced by the presence of each groove cancels from symmetry.

In a general geometry with an arbitrary (not necessarily periodic) arrangement of grooves, the far-field excess velocity is given by the limit of (16) as  $\zeta \to \infty$  combined with (10), (11). This gives a torque-free excess velocity

$$\dot{u} \sim A_{\phi} \cos \theta - B_{\phi} \sin \theta, \quad \dot{v} \sim -A_{\phi} \sin \theta - B_{\phi} \cos \theta,$$
(50)

as  $r \to \infty$ , where  $A_{\phi}$  is defined in (37) and

$$B_{\phi} = \frac{1}{\pi} \int_0^{2\pi} U(\theta') \cos \theta' \ d\theta'.$$

In Cartesian coordinates, (50) represents a streaming motion  $\hat{\bf u} \sim (A_\phi, -B_\phi)$ . Note that  $A_\phi=0$  when the distribution of grooves and ridges is symmetric about the x-axis, and  $B_\phi=0$  when it is symmetric about the y-axis. The latter occurs in (36). When the distribution is symmetric about both axes, there is even reflection symmetry about the origin and  $A_\phi=B_\phi=0$ .

For periodic structures, additional symmetries enter. Here,

$$A_{\phi} = 0 \tag{51}$$

follows from the even symmetry of  $U_N(\theta_z)$  about  $\theta_z = 0$ , while

$$B_{\phi} = \frac{1}{\pi} \left[ \sum_{k=0}^{N-1} \cos(2\pi k/N) \right] \int_{0}^{2\pi/N} U_{N}(\theta_{z}') d\theta_{z}'$$
 (52)

follows from the  $2\pi/N$  periodicity of  $U_N(\theta_z)$ . For all  $N \geq 2$  the sum is zero and  $B_\phi = 0$ . These arguments explain the absence of streaming motion for the periodic solutions constructed in Section 5, in agreement with (49).

Note the periodic symmetry is essential to the vanishing of  $A_{\phi}$ ,  $B_{\phi}$  above. Generally, when there is neither reflection symmetry about the origin nor a periodic arrangement of grooves, at least one of  $A_{\phi}$ ,  $B_{\phi}$  is nonzero, and the fluid velocity does not tend to zero at infinity. This is Jeffery's paradox for N>1.

The present problem is similar to that considered by Jeffery [14] for the counter-rotating motion of two equal cylinders in a viscous fluid. The far-field flow in [14] also consists of a streaming motion, in which the fluid is forced out in a direction perpendicular to the plane containing the axes of the cylinders, and drawn in the opposite direction.

Finally, it is interesting to note that (50) would not be observed in a model employing a homogenized or effective-slip boundary condition. The fine-scale structure of the cylinder surface is essential to Jeffery's paradox.

#### 7. Concluding remarks

We have considered the rotation of a stick–slip cylinder in a viscous fluid, as a model for the rigid-body rotation of a rough superhydrophobic cylinder. Complex variable techniques have been applied to determine all the pertinent fluid dynamic quantities, extending the study in [11]. Our analysis has been based upon transforming the flow problem into a Hilbert problem, which has been solved to obtain semi-analytic expressions for the fluid velocity and rotational mobility. Other fields, such as the pressure, can easily be determined. The solutions apply to both periodic configuration of grooves, as considered in [11], and aperiodic configurations.

A key finding in our analysis is that, for aperiodic configurations, it is generally not possible to find a solution in which the velocity of the fluid vanishes at infinity. (We have not observed that anomaly in our previous publication [11], which was exclusively focused upon periodic arrangements.) Instead, the velocity approaches a streaming motion as  $r \to \infty$ . This is a form of the Jeffery paradox [14] familiar from the counter-rotation of two equal rigid cylinders. Our work provides the first example of Jeffery's paradox due to the purely rotational motion of a single cylinder.

In his paper, Jeffery [14] refers to the observed anomaly as a form of the Stokes' paradox. It should be emphasized, however, that in the Stokes' paradox the contradiction has to do with the appearance of a velocity mode that diverges as  $\ln r$  at large distances, thus contradicting the need to approach a uniform velocity at large distances. That paradox is accordingly resolved by the incorporation of weak inertia, that enters the dominant balance at large distances. To date, comparable attempts to resolve Jeffery's paradox [20,21] have not been successful. Indeed, the resolution of Jeffery's paradox requires the removal of a uniform velocity at large distances; with that removal, small inertia is uniformly weak.

The emergence of Jeffery's paradox in the present context may be explained using the general properties of Stokes flows [22]. When a body of general geometry rotates in an unbounded fluid domain in Stokes-flow conditions, it normally experiences a hydrodynamic force. In three dimensions, such a force on a rotating stick–slip sphere is determined in [23], but unless the particle is free to translate this force is of no significance — it is merely balanced by an external force at the rotation axis. In two dimensions, however, a finite hydrodynamic force (per unit length) is associated with a velocity field that diverges as  $\ln r$  at large distances. To avoid that singularity, the mathematical solution chooses a slightly less singular behavior, by allowing for a uniform velocity at large distance. In our problem, the Stokes paradox is avoided by allowing for a Jeffery paradox!

## Declaration of competing interest

The authors declare the following financial interests/personal relationships which may be considered as potential competing interests: Michael Siegel reports financial support was provided by National Science Foundation. Ehud Yariv reports financial support was provided by Israel–US Binational Science Foundation. Michael Siegel reports financial support was provided by Israel–US Binational Science Foundation.

## Data availability

No data was used for the research described in the article

# Acknowledgments

Support is gratefully acknowledged from National Science Foundation, United States grant DMS-1909407 (M.S.) and the U.S.-Israel Binational Science Foundation grant 2020123 (M.S. and E.Y.).

#### Appendix. General solution for N grooves

## A.1. Particular solution

We derive the particular solution for N grooves with arbitrary position and arclength, closely following [16]. Let the grooves consist of N disjoint arcs  $L_1,\ldots,L_N$ , on the unit circle, and define  $L=\cup_{i=1}^N L_i$  and  $\Gamma_G=\{\theta:e^{i\theta}\in L\}$ . Define

$$F(\zeta) = \frac{1}{2\pi i} \int_{\Gamma} \frac{d\zeta'}{\zeta'} \frac{\zeta' + \zeta}{\zeta' - \zeta} \, \hat{U}(\zeta'),\tag{53}$$

which clearly represents an analytic function in  $\mathbb{C}-L$ . Let  $F_i(\theta)$  (respectively  $F_o(\theta)$ ) denote the value of  $F(\zeta)$  as  $\zeta \to e^{i\theta} \in L$  from inside (respectively outside) L. Using contour deformation, it is easily seen that

$$F_i(\theta) - F_o(\theta) = 2\hat{U}(\theta),\tag{54}$$

$$F_i(\theta) + F_o(\theta) = \frac{1}{\pi i} \text{PV} \int_{\Gamma_o} \hat{U}(\theta') \cot\left(\frac{\theta' - \theta}{2}\right) d\theta'$$
 (55)

$$= -2iB_k(\theta), \tag{56}$$

for  $\theta \in L_k$ , where in the last equality we have used (22). This is the Riemann problem: to find a function given a linear relation between its values on the inside and outside of a curve.

Now, let  $\alpha_k$  and  $\beta_k$  denote the beginning and end of the arc  $L_k$  (traversed counterclockwise) and introduce

$$\omega(\zeta) = \prod_{k=1}^{N} \left( \frac{\zeta - \alpha_k}{\zeta - \beta_k} \right)^{1/2}$$

where the branch cuts are taken along the  $L_k$ . Define a function  $\Phi(\zeta)$  by

$$F(\zeta) = \omega(\zeta)\Phi(\zeta). \tag{57}$$

Substitute (57) into (55) and use  $\omega_i(\theta) + \omega_o(\theta) = 0$  to find

$$\boldsymbol{\varPhi}_{i}(\theta) - \boldsymbol{\varPhi}_{o}(\theta) = -\frac{2iB_{k}(\theta)}{\omega_{i}(\theta)}, \label{eq:phi_equation}$$

for  $\theta \in L_k$ . Inspection of (53) and (54) suggests that

$$\varPhi(\zeta) = -\frac{1}{2\pi} \int_L \frac{d\zeta'}{\zeta'} \frac{\zeta' + \zeta}{\zeta' - \zeta} \ \frac{B_k(\zeta')}{\omega_i(\zeta')},$$

where the function  $B_k$  is used when integration is along the arc  $L_k$ . It follows that

$$F(\zeta) = -\frac{\omega_i(\zeta)}{2\pi} \int_L \frac{d\zeta'}{\zeta'} \frac{\zeta' + \zeta}{\zeta' - \zeta} \frac{B_k(\zeta')}{\omega_i(\zeta')}.$$

Henceforth we omit the subscript i on  $\omega$ . Expressions for  $F_i(\theta)$  and  $F_o(\theta)$  are determined from the above by contour deformation, from which (54) gives for  $\zeta \in L$ 

$$\hat{U}(\zeta) = -\frac{\omega(\zeta)}{2\pi} \, \text{PV} \int_{I} \frac{d\zeta'}{\zeta'} \frac{\zeta' + \zeta}{\zeta' - \zeta} \, \frac{B_k(\zeta')}{\omega(\zeta')},$$

or equivalently

$$\hat{U}(\theta) = -\frac{\omega(\theta)}{2\pi} \text{ PV} \int_{\Gamma_G} \frac{B_k(\theta')}{\omega(\theta')} \cot\left(\frac{\theta' - \theta}{2}\right) d\theta'.$$
 (58)

for  $\theta \in \Gamma_G$ 

Note that (58) remains a particular solution when  $\omega^{-1}$  is substituted for  $\omega$ . This gives the symmetric form

$$\begin{split} \hat{U}(\theta) &= -\frac{\omega(\theta)}{4\pi} \, \text{PV} \int_{\Gamma_G} \frac{B_k(\theta')}{\omega(\theta')} \cot\left(\frac{\theta' - \theta}{2}\right) \, d\theta' \\ &- \frac{1}{4\pi\omega(\theta)} \, \text{PV} \int_{\Gamma_G} B_k(\theta') \omega(\theta') \cot\left(\frac{\theta' - \theta}{2}\right) \, d\theta', \end{split}$$

for  $\theta \in \Gamma_G$ , which in the case N = 1 is the particular solution in (25).

#### A.2. Homogeneous solution

We derive all solutions  $\hat{U}_h$  to the homogeneous Eq. (28) for N grooves, following [16]. Consider the function  $F(\zeta)$  in (53) with  $\hat{U}=\hat{U}_h$ , which we denote by  $F_h$ . We require  $\hat{U}_h$  to be integrable on L so that

$$\lim_{\zeta \to \infty} F_h(\zeta) = -\frac{1}{2\pi} \int_{\varGamma_G} \hat{U}_h(\theta) \ d\theta.$$

is finite. Let  $\Phi_h$  be defined as in (57), and note that this function is bounded as  $\zeta \to \infty$  and satisfies the equation

$$\Phi_{hi}(\theta) - \Phi_{ho}(\theta) = 0$$

for  $\theta \in \Gamma_G$ . Since  $\Phi_h$  takes the same values on both sides of L, it follows that this function is regular in the entire plane, except possibly at  $\alpha_k$  and  $\beta_k$ . An argument given in Mikhlin [16] then shows that the  $\beta_k$ 's are regular points of  $\Phi_h$  and the  $\alpha_k$ 's are either regular points or simple poles.

The above arguments show that the most general form for  $\Phi_h$  having the correct behavior at infinity is

$$\boldsymbol{\Phi}_{h}(\zeta) = \frac{\sum_{k=0}^{N} a_{k} \zeta^{k}}{\prod_{k=1}^{N} (\zeta - a_{k})}$$
(59)

for  $a_k \in \mathbb{C}$ . Thus,

$$F_h(\zeta) = \frac{\sum_{k=0}^{N} a_k \zeta^k}{\prod_{k=1}^{N} \left[ (\zeta - \alpha_k)(\zeta - \beta_k) \right]^{1/2}}$$
 (60)

and  $\hat{U}_h$  is given by (54) combined with  $F_{hi}(\theta) = -F_{ho}(\theta)$ . Examination of the limiting behavior of  $F_h(\zeta)$  as  $\zeta \to \infty$  and  $\zeta \to 0$  provides the constraint

$$a_N = -\frac{a_0}{\prod_{k=1}^{N} (\alpha_k \beta_k)^{1/2}}.$$
(61)

The 2N free constants,  $a_k$  for  $k=0,\ldots,N-1$  and  $C_k$  for  $k=1,\ldots,N$  (the constants of integration in (15)) are chosen to enforce  $\hat{U}_p + \hat{U}_h = 0$  at  $\alpha_k, \beta_k$  for  $k=1,\ldots,N$ . The remaining condition (17) determines T.

When N=1 (cf. Section 4) we set  $\alpha_1=\alpha$ ,  $\beta_1=-\bar{\alpha}$ , and  $a_0=-Di$  so that from (61)  $a_1=D$ . The comment following (60) then shows that the homogeneous solution  $\hat{U}_h$  is given by (29).

#### References

- S. Parvate, P. Dixit, S. Chattopadhyay, Superhydrophobic surfaces: Insights from theory and experiment, J. Phys. Chem. B 124 (8) (2020) 1323–1360.
- [2] D. Quéré, Wetting and roughness, Annu. Rev. Mater. Res. 38 (2008) 71-99.
- [3] L. Bocquet, E. Lauga, A smooth future? Nature Mater. 10 (5) (2011) 334-337.

- [4] D. Crowdy, Slip length for longitudinal shear flow over a dilute periodic mattress of protruding bubbles, Phys. Fluids 22 (12) (2010) 121703.
- [5] A. Davis, E. Lauga, Hydrodynamic friction of Fakir-like superhydrophobic surfaces, J. Fluid Mech. 661 (2010) 402–411.
- [6] J.R. Philip, Flows satisfying mixed no-slip and no-shear conditions, ZAMP 23 (1972) 353–372.
- [7] E. Lauga, H.A. Stone, Effective slip in pressure-driven Stokes flow, J. Fluid Mech. 489 (2003) 55–77.
- [8] M. Castagna, N. Mazellier, A. Kourta, Wake of super-hydrophobic falling spheres: Influence of the air layer deformation, J. Fluid Mech. 850 (2018) 646–673.
- [9] A. Jetly, I. Vakarelski, S. Thoroddsen, Drag crisis moderation by thin air layers sustained on superhydrophobic spheres falling in water, Soft Matter 14 (9) (2018) 1608–1613.
- [10] P. Muralidhar, N. Ferrer, R. Daniello, J. Rothstein, Influence of slip on the flow past superhydrophobic circular cylinders, J. Fluid Mech. 680 (2011) 459–476.
- [11] E. Yariv, M. Siegel, Rotation of a superhydrophobic cylinder in a viscous liquid, J. Fluid Mech. 880 (2019) R4.
- [12] M. Siegel, Influence of surfactant on rounded and pointed bubbles in two-dimensional Stokes flow, SIAM J. Appl. Math. 59 (6) (1999) 1998–2027.
- [13] D. Crowdy, Surfactant-induced stagnant zones in the Jeong-Moffatt free surface Stokes flow problem, Phys. Fluids 25 (9) (2013) 092104.
- [14] G. Jeffery, The rotation of two circular cylinders in a viscous fluid, Proc. R. Soc. Lond. Ser. A 101 (709) (1922) 169–174.
- [15] E. Dormy, H. Moffatt, Flow induced by the rotation of two circular cylinders in a viscous fluid, 2020, arXiv preprint arXiv:2008.04432.
- [16] S.G. Mikhlin, Integral Equations and their Applications To Certain Problems in Mechanics, in: Mathematical Physics and Technology, vol. 4, Elsevier, 2014.
- [17] W.E. Langlois, M.O. Deville, Slow Viscous Flow, Springer, 1964.
- [18] B.K. Alpert, Hybrid Gauss-trapezoidal quadrature rules, SIAM J. Sci. Comput. 20 (5) (1999) 1551–1584.
- [19] O.E. Jensen, D. Halpern, The stress singularity in surfactant-driven thin-film flows. Part 1. Viscous effects, J. Fluid Mech. 372 (1998) 273–300.
- [20] S.H. Smith, The rotation of two circular cylinders in a viscous fluid, Mathematika 38 (1) (1991) 63–66.
- [21] E.J. Watson, The rotation of two circular cylinders in a viscous fluid, Mathematika 42 (1) (1995) 105–126.
- [22] J. Happel, H. Brenner, Low Reynolds Number Hydrodynamics, Prentice-Hall, Englewood Cliffs, N. J. 1965
- [23] A. Premlata, H.-H. Wei, Coupled Faxen relations for non-uniform slip Janus spheres, Phys. Fluids 33 (11) (2021) 112003.